LA-UR- 12-00799

Approved for public release;
distribution is unlimited.

Title:	Cercion: A Material Strength ALE Code with a Higher-Order Remap using Flux Volume Centroids
Author(s):	Vincent Chiravalle
Intended for:	Submission to Computers and Fluids

Los Alamos
NATIONAL LABORATORY
EST. 1943

Form 836 (7/06)

Cercion: A Material Strength ALE Code with a Higher-Order Remap using Flux Volume Centroids

Vincent P. Chiravalle

Los Alamos National Laboratory

Abstract

A numerical technique for solving the equations of fluid dynamics for multimaterial flows with arbitrary mesh motion in two dimensional cylindrical geometry was implemented in an ALE hydrodnamics code called Cercion, written in the C programming language using novel cell-centered data structures. The Lagrangian phase follows a well known approach using a spatial and temporal staggered grid. The remap phase includes a higher order correction to the donor cell method that is calculated using the true geometric centers of the flux volumes. Five test problems were explored to evaluate the fidelity of the numerical techniques in Cercion. The locations of the shock and contact discontinuity in the Sod shock tube problem on a fixed mesh are well captured and results from Cercion are compared with those from four other Eulerian numerical methods. Cercion demonstrates a high degree of symmetry when calculating the Sedov blast wave solution in pure Lagrangian mode. When calculating the cylindrical implosion of a steel shell, the Cercion solution is insensitive to the the use of ALE.

Keywords: Hydrodynamics Methods

1. Introduction

The field of Arbitrary Lagrangian Eulerian (ALE) hydrodynamics has enjoyed a long and fruitful development. ALE is an indispensible tool for researchers studying energetic materials, plasmas, and turbulence among many other applications. There are two parts to ALE: the relaxation of the computational mesh and the remapping of mass, energy and momentum onto the new mesh. Various approaches for both mesh relaxation and remapping have been explored in the literature. An excellent summary of the various methods is given by Benson [1]. One of the first ALE codes for two dimensional cylindrical geometry was SALE [2] which implemeneted a simplified version of the algorthim proposed by Hirt et al. [3] that is applicable to both compressible and incompressible flows. SALE solves the hydrodynamic equations in three sequential phases: a Lagrangian phase, a mesh relaxation phase and a remap phase. The momentum equations and the internal energy equations are updated during the Lagrangian phase in a manner similar to other purely Lagrangian codes such as HEMP [4]. In HEMP the material strength treatment first involves finding the flow strains from the velocity field, updating the von Mises flow stress using an appropriate model such as the PTW model [5] or the Steinberg model [6], and then finally using the updated flow stress together with a yield surface criterion to find the stress deviator components. Unlike HEMP, SALE does not utilize material strength. Subsequent to the development of SALE, a similar code was formulated, SHALE [7], which not only incorporated ALE but also had an improved strength treatment relative to HEMP. Both HEMP and SHALE solve the fluid equations in a two dimensional geometry with cylindrical symmetry and there are four components of the stress deviator tensor with three of these being independent. The stress deviator components enter into the momentum equation and the stress related work term enters into the energy equation. During the Lagrangian phase in SALE the momentum equations are solved on a grid that is staggered spatially with respect to the corresponding grid for the cell-centered quantities such as mass, energy and the stress deviator components. This staggered grid arrangement is also used in HEMP. In addition to spatial staggering, the vertex-center velocities are also temporally staggered in HEMP. Having obtained new values for velocity after the Lagrangian phase, SALE then updates the positions of the vertices on the mesh. At this point mesh relaxation is considered and SALE has three options: maintain the Lagrangian positions, remap to

the initial mesh positions (Eulerian method) or remap to positions corresponding to a user specified weight between these two extremes. As research in ALE methods continued and as ALE codes began to be more widely applied, sophisticated techniques were developed for mesh relaxation. Contemporary methods involve the optimization of a global integral relating to smoothness, orthogonal nature of the grid lines, and other properties of the mesh, as described by Brackbill and Saltzman [8]. Minimizing the integral involves a few iterations on the vertex positions each cycle using the conjugate gradient technique. An exact solution for the optimum vertex positions is not obtained at any given cycle but with time the mesh converges to the optimum solution. A simpler alternative to a global optimization method is the regular use of a finite difference vertex relaxer such as the one proposed by Winslow [9] which adjusts the vertex points locally using only the positions of neighboring vertices to achieve an equipotential mesh in an iterative fashion after many cycles.

The task of remapping the physical quantities from the old mesh to the new mesh is performed during the remap phase. SALE utilizes a first order donor-cell method for the mass and energy remap. The donor cell method involves determining flux volumes for each side of the cell associated with the movement of material from the old to the new mesh, and assigning a material density and energy density to these volumes. It is well known that first-order methods do not preserve sharp gradients as discussed by Laney [10] and therefore these methods are rarely used in ALE codes. Higher-order remap methods have been developed and two good examples are the second order sign-preserving method of Margolin and Shaskov [11] and the Barth-Jespersen method [12]. These higher order methods add corrections to the fluxes computed by the donor-cell method. In particular the Barth-Jespersen method constructs a density gradient at each cell center, suitably limited to preserve monotonicity. For each remapped quantity the appropriate density gradient is used to construct the flux, be it a mass or energy. Cercion incorporates a new and simpler way to contruct the fluxes for the remap using the monotone gradients from the Barth-Jespersen method.

Both SALE and SHALE do not allow remapping across material interfaces; it is assumed that material interfaces always evolve in a Lagrangian fashion. This assumption can be problematic in many situations where turbulence arises. One way to circumvent this difficulty is to use an interface reconstruction technique such as the one developed by Youngs [13]. Youngs' volume of fluid (VOF) method represents a material interface in a piecewise linear fashion. In each cell there are three parameters describing the local straight line representation of the interface. The slope of the line is determined by the local volume fraction gradient and its position relative to the cell center is determined to match the volume of material in the cell. Additional computational details of the VOF method and a description of other alternate methods for interface reconstruction are given by Kucharik et al. [14] and Morgan [15].

A central issue for any code that solves the equations of hydrodynamics, be it Lagrangian, Eulerian or ALE, is the type of artificial viscosity employed to capture non-linear discontinuities such as shock waves. Since its introduction in 1950 by von Neumann and Richtmyer [16], the scalar artificial viscosity, with a quadratic dependence on velocity difference has been ubiquitous in the CFD literature. The corresponding artificial stress term is added to the pressure in the momentum equation to suppress numerical oscillations in regions with strong shocks. Bowers and Wilson [17] describe how to implement the scalar artificial viscosity in a two dimensional, cylindrically symmetric Eulerian code. In this case the radial and axial components are treated separately but analogously and the two components of artificial viscosity each have both a quadratic term and a linear term. Wilkins [18] gives an excellent discussion of a tensor artificial viscosity in a two dimensional cylindrical geometry and Christiansen [19] describes a higher order flux-limited artificial viscosity.

A new ALE hydrodynamics code called Cercion is described in this paper that uses the proven Lagrangian scheme from HEMP and a higher order remap technique incorporating not only cell-centered monotone gradients but also flux volume centroids. The present remap approach can be used together with the VOF method for material interfaces in mixed cells. The details of the numerical implementation are discussed in Section 2, including the novel cell-centered data structures that are used in Cercion to reduce the complexity of the programming and maximize the efficiency of memory usage. In Section 3, a series of three test problems are considered to validate Cercion; these problems include the Sod shock tube, the Sedov blast wave and the aluminum flyer plate. Comparisons are made with analytic solutions and calculations using another Lagrangian hydrodynamics code. The cylindrical implosion of a steel shell with material strength is studied in Section 4, and calculations are performed both in pure Lagragian mode and using ALE. In addition the Verney test problem involving the spherical implosion of an incompressible steel shell is also explored. Finally a summary and conclusions are presented in Section 5.

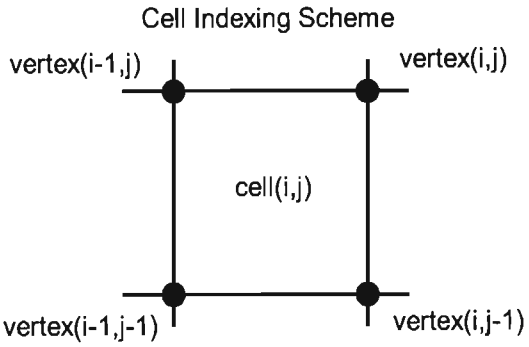

Figure 1: Cell and vertex indexing scheme.

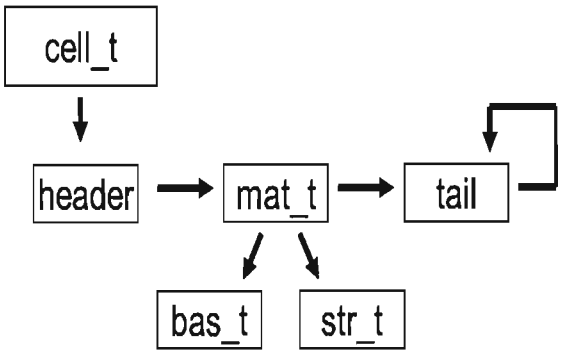

Figure 2: Linked list for a cell with 1 material.

2. Numerical Implementation

Cercion follows a numerical implementation of the ALE technique that is similar to SALE but there are some key differences and additional features. The hydrodynamics is solved on a block-structured mesh where each mesh block contains only quadrilateral cells arranged in a regular fashion. A given mesh block has four faces and four corner points. The user specifies in the input file how each of the mesh blocks is connected to the other blocks in terms of the boundary faces and corners. Velocities are stored at the vertices of the cell, whereas density and pressure are stored at the cell center. The indexing convention for a cell is shown in Fig. 1. Cercion was written using the ANSI standard C programming language, with a Fortran style of indexing for the array data structures. There are three essential elements to the numerical implementation in Cercion: the cell-centered data structures, the Lagrangian phase velocity update, and the higher order remap method.

The data structures in Cercion are cell-oriented. Each cell is represented by a composite data type, cell_t, including a dynamic material list as well as storage for all of the cell-centered quantities, such as mass, pressure and specific energy, and storage for the position and velocity components of the top-right vertex (i,j) associated with the cell. With this data type, information related to the cell can be obtained without searching various disparate and unconnected arrays.

An example of a dynamic linked list of materials is given in Fig. 2. Within the linked list there is a single element for each material in the cell; a composite data type, mat_t, is used to store all the information for a given material. The elements in the dynamic material list are ordered according to the onion skin method [20]. Each element points to two other data types, bas_t and str_t as illustrated in Fig. 2. Basic material properties including volume fraction, mass, energy, density, density derivatives, and VOF interface parameters are stored in the bas_t data structure. For materials that have strength, strength properties are stored in the str_t data structure. Strength properties encompass stress deviator components, equivalent plastic strain, and the derivatives associated with these quantities. In addition to a dynamic material list, the cell_t data structure also contains pointers to two other linked lists, one associated with the top boundary of the cell and another associated with the right boundary. These two material flux linked lists each contain information about the materials crossing the associated cell boundary.

The first part of the hydrodynamic solution involves solving for the updated velocity components using the Lagrangian algorithm from HEMP which constructs a control volume around vertex (i,j) that resembles a diamond with the faces of the diamond passing through the centers of cells A, B, C, and D as shown in Fig. 3. The corners of the diamond are the four neighboring vertices. The finite difference equation for the axial velocity component, u, is given in Eqn. 1 and the radial component, v, in Eqn. 2. The values of the Cauchy stress tensor components, stored at the cell centers, are used to update the velocity components. The Cauchy stress tensor, Σ, includes the pressure, the stress deviators and the artificial viscous stress for numerical stability. In a cylindrical geometry there are additional contributions to the velocity equations from the stress deviator tensor proportional to $1/r$; these are denoted as α and β in Eqn. 1 and Eqn. 2. An area-weighted scheme is used in HEMP for calculating these terms as illustrated below. The same method is applied in Cercion but the true mass of a cell over the complete solid angle is used, whereas

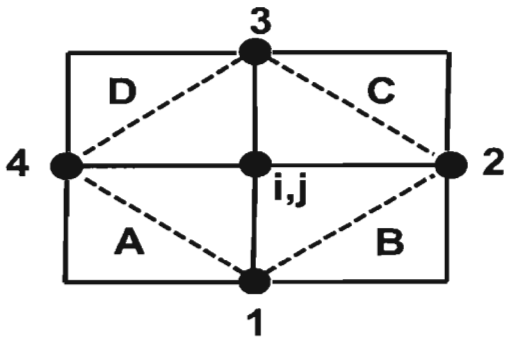

Figure 3: HEMP control volume for the velocity at vertex (i,j).

HEMP does not use the true mass, hence the $\pi/2$ factor. The corresponding difference equations in HEMP have a factor of 1/4 instead.

$$\begin{aligned} u_{i,j}^{n+1} &= u_{i,j}^{n} \\ &- \frac{\Delta t}{2\phi_{i,j}}\left[\Sigma_{xx}^{A}(y_4 - y_1) + \Sigma_{xx}^{B}(y_1 - y_2)\right] \\ &- \frac{\Delta t}{2\phi_{i,j}}\left[\Sigma_{xx}^{C}(y_2 - y_3) + \Sigma_{xx}^{D}(y_3 - y_4)\right] \\ &+ \frac{\Delta t}{2\phi_{i,j}}\left[\Sigma_{xy}^{A}(x_4 - x_1) + \Sigma_{xy}^{B}(x_1 - x_2)\right] \\ &+ \frac{\Delta t}{2\phi_{i,j}}\left[\Sigma_{xy}^{C}(x_2 - x_3) + \Sigma_{xy}^{D}(x_3 - x_4)\right] \\ &+ \Delta t \alpha_{i,j} \end{aligned} \tag{1}$$

$$\begin{aligned} \phi_{i,j} &= \frac{1}{4}\left[(\rho A)_A + (\rho A)_B + (\rho A)_C + (\rho A)_D\right] \\ \alpha_{i,j} &= \frac{\pi}{2}\left[\left(\frac{\Sigma_{xy}A}{M}\right)_A + \left(\frac{\Sigma_{xy}A}{M}\right)_B\right] \\ &+ \frac{\pi}{2}\left[\left(\frac{\Sigma_{xy}A}{M}\right)_C + \left(\frac{\Sigma_{xy}A}{M}\right)_D\right] \end{aligned}$$

$$\begin{aligned} v_{i,j}^{n+1} &= v_{i,j}^{n} \\ &+ \frac{\Delta t}{2\phi_{i,j}}\left[\Sigma_{yy}^{A}(x_4 - x_1) + \Sigma_{yy}^{B}(x_1 - x_2)\right] \\ &+ \frac{\Delta t}{2\phi_{i,j}}\left[\Sigma_{yy}^{C}(x_2 - x_3) + \Sigma_{yy}^{D}(x_3 - x_4)\right] \\ &- \frac{\Delta t}{2\phi_{i,j}}\left[\Sigma_{xy}^{A}(y_4 - y_1) + \Sigma_{xy}^{B}(y_1 - y_2)\right] \\ &- \frac{\Delta t}{2\phi_{i,j}}\left[\Sigma_{xy}^{C}(y_2 - y_3) + \Sigma_{xy}^{D}(y_3 - y_4)\right] \\ &+ \Delta t \beta_{i,j} \end{aligned} \tag{2}$$

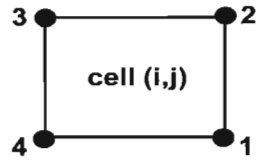

Figure 4: Vertices used to calculate the strain rate for cell (i,j).

$$\begin{aligned} \beta_{i,j} &= \frac{\pi}{2}\left[\left(\frac{\Sigma_{yy} - \Sigma_{\theta\theta}}{M}A\right)_A + \left(\frac{\Sigma_{yy} - \Sigma_{\theta\theta}}{M}A\right)_B\right] \\ &+ \frac{\pi}{2}\left[\left(\frac{\Sigma_{yy} - \Sigma_{\theta\theta}}{M}A\right)_C + \left(\frac{\Sigma_{yy} - \Sigma_{\theta\theta}}{M}A\right)_D\right] \end{aligned}$$

Prior to solving the velocity equations, the stress deviator components are updated from the previous cycle using the strain rate components. Cercion does not use the HEMP methodology for calculating the strain rate components but rather the method proposed by Margolin [21] is adopted, whereby the flow divergence is calculated in a manner that is consistent with the strain rate. The strain rate components, $\dot{\epsilon_{xx}}$, $\dot{\epsilon_{yy}}$, $\dot{\epsilon_{\theta\theta}}$, and $\dot{\epsilon_{xy}}$ are given by Eqn. 3, Eqn. 4, Eqn. 5, and Eqn. 6, respectively. Fig. 4 identifies the vertices that are used in the calculation of the strain rate components. The calculation of the strain rate components relies on area and radius terms denoted A_{ijk} and r_{ijk} in Eqn. 3, where the subscripts i,j,k span the four vertices surrounding the cell in Fig. 4. The Margolin approach employs a volume averaged approximation to the spatial velocity derivatives whereas the HEMP approach uses an area averaged approximation. Margolin demonstrates that in certain situations the area averaged method is not a good approximation to the true strain rate.

$$\begin{aligned} \dot{\epsilon_{xx}} &= \frac{1}{6V}\left[(u_3 r_{234} - u_1 r_{412})(y_2 - y_4)\right] \\ &+ \frac{1}{6V}\left[(u_4 r_{341} - u_2 r_{123})(y_3 - y_1)\right] \\ V &= \frac{1}{6}\left[r_{123}A_{123} + r_{234}A_{234}\right] \\ &+ \frac{1}{6}\left[r_{341}A_{341} + r_{412}A_{412}\right] \\ A_{ijk} &= \frac{1}{2}\left[(y_k - y_j)(x_i - x_j)\right] \\ &- \frac{1}{2}\left[(y_i - y_j)(x_k - x_j)\right] \\ r_{ijk} &= y_i + y_j + y_k \end{aligned} \tag{3}$$

$$\dot{\epsilon_{yy}} = \frac{1}{6V}\left[(v_1 r_{412} - v_3 r_{234})(x_2 - x_4)\right]$$

$$+ \frac{1}{6V}\left[(v_2 r_{123} - v_4 r_{341})(x_3 - x_1)\right]$$
$$- \frac{1}{6V}(v_1 A_{412} + v_2 A_{123})$$
$$- \frac{1}{6V}(v_3 A_{234} + v_4 A_{341}) \quad (4)$$

$$\dot{\epsilon}_{\theta\theta} = \frac{1}{2V}(v_1 A_{412} + v_2 A_{123})$$
$$+ \frac{1}{2V}(v_3 A_{234} + v_4 A_{341}) \quad (5)$$

$$\dot{\epsilon}_{xy} = \frac{1}{6V}\left[(v_3 r_{234} - v_1 r_{412})(y_2 - y_4)\right]$$
$$+ \frac{1}{6V}\left[(v_4 r_{341} - v_2 r_{123})(y_3 - y_1)\right]$$
$$+ \frac{1}{6V}\left[(u_1 r_{412} - u_3 r_{234})(x_2 - x_4)\right]$$
$$+ \frac{1}{6V}\left[(u_2 r_{123} - u_4 r_{341})(x_3 - x_1)\right]$$
$$- \frac{1}{6V}(u_1 A_{412} + u_2 A_{123})$$
$$- \frac{1}{6V}(u_3 A_{234} + u_4 A_{341}) \quad (6)$$

$$\nabla \cdot U = \epsilon_{xx} + \epsilon_{yy} + \epsilon_{\theta\theta} \quad (7)$$

Besides being more versatile than other methods, the volume averaged technique of Margolin also has the desirable property that the flow divergence can be calculated from the strain rate components exactly as shown in Eqn. 7, without introducing additional errors into the finite difference equations. The flow divergence is required to calculate the change in internal energy during the Lagrangian phase and it is also used to determine the artificial viscous stress as given in Eqn. 8. The internal energy update performed in Cercion is the two-step process borrowed from HEMP, where the equation of state is evaluated twice for pressure during the update.

$$q = \rho\left[C_2 A(\nabla \cdot U)^2 - C_1 \sqrt{A} a(\nabla \cdot U)\right] \quad (8)$$

There are two components in Eqn. 8 for the artificial viscous stress, one a linear term in flow divergence and the other a quadratic term. This form of artificial viscous stress is scalar in nature and the artificial viscous stress only appears in two of the Cauchy stress tensor components, Σ_{xx} and Σ_{yy}, as opposed to affecting all components. The two component formulation from Eqn. 8, where a is the sound speed, is a straightforward way to generalize the von Neumann viscous stress intended for one dimensional problems into two dimensions; this linear-quadratic formulation was used in later versions

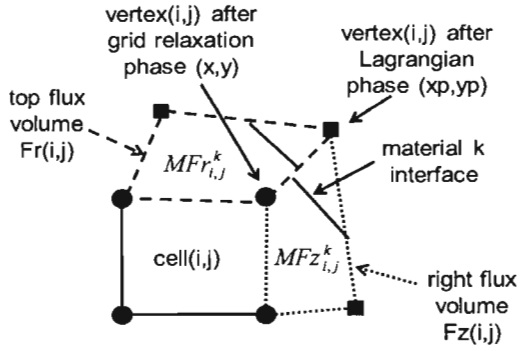

Figure 5: Flux volumes for cell (i,j).

of HEMP as described by Wilkins [18]. All the calculations in this paper have coefficients of $C_2 = 2.0$ and $C_1 = 0.1$ for the quadratic and linear terms respectively. Cercion uses the simple finite difference mesh relaxer proposed by Winslow with a nine point stencil [9]. The user can specify in the input file whether any particular set of vertices are relaxed and the time interval for the relaxation. During the remap phase material fluxes are used to redistribute materials among cells whose vertices have been relaxed. Fig. 5 illustrates a cell containing two materials where three of the cell vertices have been relaxed. The vertex positions after the Lagrangian phase (xp, yp) are denoted with squares and the relaxed positions (x, y) with circles. The flux volume through the top face, Fr, and the flux volume through the right face, Fz, both of which are positive in Fig. 5, are calculated by determining the path integral in a counterclockwise direction along the vertex positions that comprise the flux volume. For multimaterial cells the flux volumes are partitioned to represent the individual material fluxes using the appropriate piece-wise linear interface; the mass of material k contained in the flux volume Fz is denoted MFz^k in Fig. 5. MFz^k is determined using the donor cell technique as presented in Eqn. 9.

$$MFz^k_{i,j} = \rho^k_{up} Fz^k_{i,j} \quad (9)$$

The donor cell technique uses the upwind density for material k, ρ^k_{up} such that if the material flows out of cell (i,j) and the flux volume $Fz^k_{i,j}$ is positive then the density from cell (i,j) is taken as the upwind density otherwise the density from cell(i+1,j) is the upwind density. The update of material k mass from the Lagrangian value, M^k, to the value after the remap step, M^{k*}, is performed as shown in Eqn. 10. Mass fluxes from four neighboring cells are used to update the material k mass. An

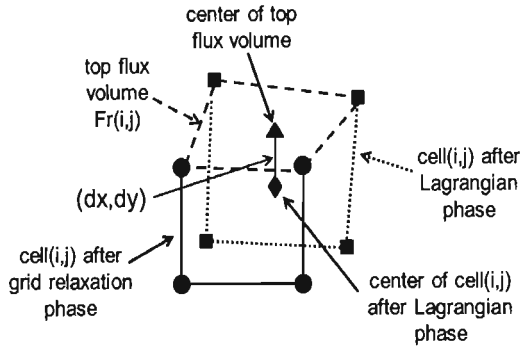

Figure 6: Flux volumes for cell (i,j).

analogous equation is solved for the material k internal energy and other cell-centered quantities.

$$M^{k*}_{i,j} = M^{k}_{i,j} - \left[MFz^{k}_{i,j} - MFz^{k}_{i-1,j}\right] - \left[MFr^{k}_{i,j} - MFr^{k}_{i,j-1}\right] \quad (10)$$

In Cercion, a second order correction is made to the donor cell method for those cells with a single material. The method for calculating the higher order correction involves the geometric centers of the flux volume and is displayed in Fig. 6 for the material mass flux crossing the top boundary of cell (i,j). The cell volume after the Lagrangian phase and cell volume after the mesh relaxation phase are illustrated as they relate to the top flux volume. The geometric centers of the top flux volume and the Lagrangian volume of the cell are highlighted in Fig. 6 as triangles. The distance between the centers (dx, dy) is used together with the upwind density derivatives in a straightforward way to achieve a higher order mass flux given by Eqn 11.

$$MFr_{i,j} = \rho_{up} Fr_{i,j} + Fr_{i,j}\left[dx\left(\frac{\partial \rho}{\partial x}\right)_{up} + dy\left(\frac{\partial \rho}{\partial y}\right)_{up}\right] \quad (11)$$

Density derivatives are calculated at the cell centers using the Barth-Jespersen approach involving a control volume formed from all eight neighboring cells [12]. The Barth-Jespersen method also imposes a limit on the value of each derivative to ensure a monotone flow. The limiting function proposed by Barth and Jespersen is used in Cercion to the same effect. The upwind density derivatives assigned to the material fluxes are determined from the Barth-Jespersen derivates at the cell centers using the same upwind approach associated with Eqn. 9.

The mass fluxes calculated during the remap of the cell-centered quantities are retained for use during the momentum remap; this was inspired by the approach of Bowers and Wilson [17]. In addition to the cell-centered quantities a higher order remap of the form of Eqn. 11 is also used for momentum but the momentum control volume is vertex-centered, and the momentum flux volumes are different owing to the spatially staggered nature of the Lagrangian method used in Cercion.

3. Basic Test Problems

Having described the fundamental algorithms, in this section Cercion is tested with a series of simple problems in both one and two dimensions. The Sod shock tube was used to assess the fidelity in capturing shocks and contact discontinuities. The degree of symmetry in the code solution was tested with a Sedov blast wave problem and the ability to calculate the elastic-plastic response in one dimension was evaluated with an aluminum flyer plate problem.

The Sod shock tube is common in the CFD literature and since there is an analytic solution it is a good test of the basic conservation properties of any numerical fluid dynamics algorithm [22]. An initial discontinuity between two ideal gas regions ($\gamma = 5/3$) exists at time zero. The first region has a density of 1 kg/m^3 and a pressure of 1 N/m^2. The second region has a density of 0.125 kg/m^3 and a pressure of 0.1 N/m^2. There is a contact discontinuity at the interface between the two regions, which moves as the problem progresses. An Eulerian mesh consisting of a uniform box 0.1 m by 1 m having 2 radial zones and 100 axial zones was used for the Cercion simulation. The numerical solution at 0.1415s for the density and pressure is given in Fig. 7 and Fig. 8, together with the analytic solution. The location of the contact discontinuity at about 0.6 m is well captured by the simulation. An expansion fan is also visible in the numerical solution for both pressure and density, agreeing nicely with the analytic solution. Simulation results for this test problem using four other Eulerian numerical techniques are also presented; these numerical techniques include the TVD MacCormack scheme [23], the flux vector splitting scheme of Van Leer [24], the method proposed by Bowers and Wilson [17], and the FLIC method developed by Gentry et al. [25]. In comparison to these other methods Cercion does about as well in representing the contact discontinuity and expansion fan. While the other four methods capture the shock wave in three zones, Cercion is more dissipative with the shock being spread over at least six zones as best illustrated by the spatial profile of velocity

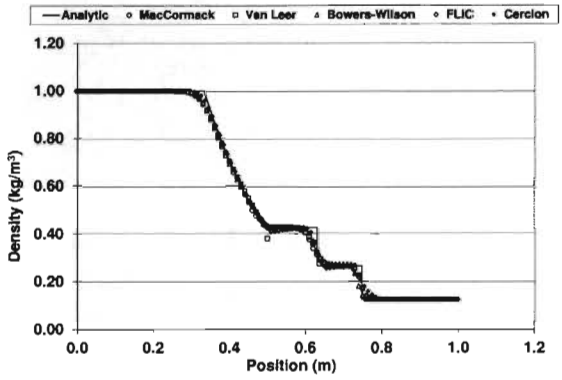

Figure 7: Density for the shock tube problem.

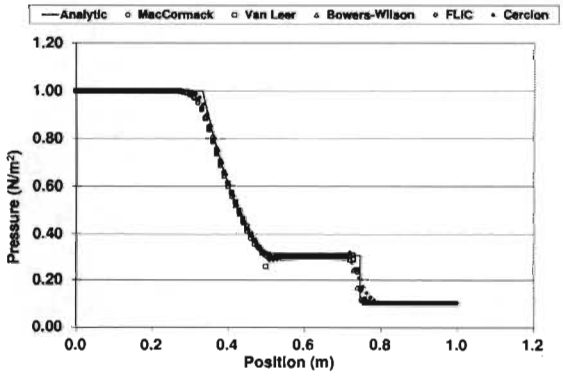

Figure 8: Pressure for the shock tube problem.

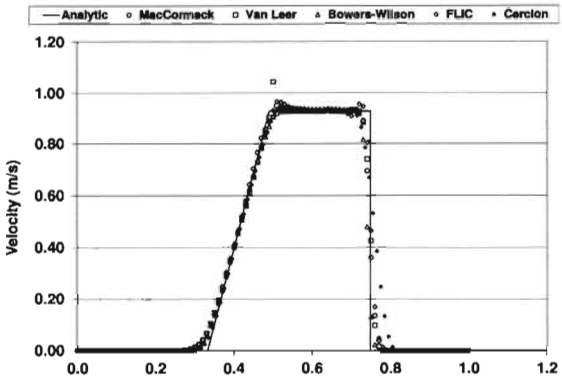

Figure 9: Velocity for the shock tube problem.

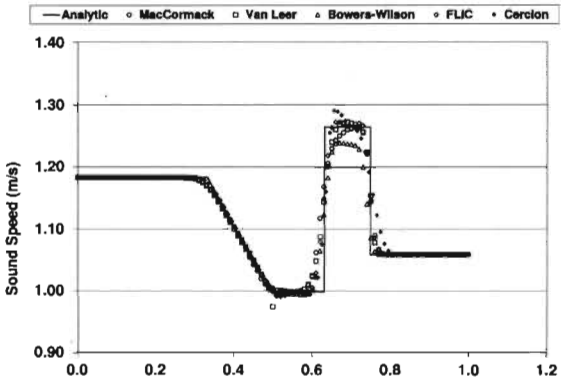

Figure 10: Sound speed for the shock tube problem.

in Fig. 9. The sound speed spatial profile has the most variation among the five methods as shown in Fig. 10. Cercion gives a slight overshoot of about 2% in front of the contact discontinuity whereas the Bowers and Wilson method produces a sound speed that is about 2% less than the analytic solution between the contact discontinuity and the shock. Overall Cercion does a good job in capturing the details of the expansion fan and the contact discontinuity, but with regard to the shock it produces a more diffuse result than the other advection methods.

The Sedov blast wave problem involves the propagation of a strong disturbance arising from a localized energy source of 52 kJ at the origin. As time progresses a self-similar solution is obtained that is spherically symmetric. In a two dimensional cylindrical geometry, the Sedov blast wave is a good way to evaluate the symmetry preserving properties of the numerical algorithm. A calculation in pure Lagrangian mode was performed on a uniform mesh with 193 axial zones and 96 radial

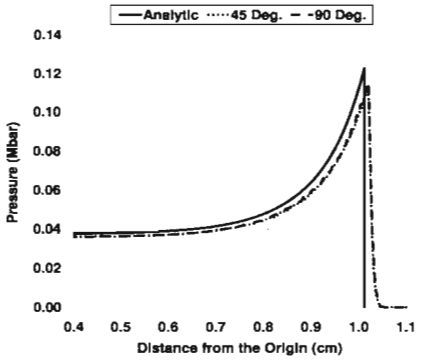

Figure 11: Density for the Sedov test problem.

zones; the resolution in both directions was 125 μm. The energy source is contained entirely within a single zone with the origin at the center of that zone. For this test problem the solution is obtained at 1 μs and the time step is fixed at $10^{-5}\mu$s. Furthermore an additional artifical viscous stress, separate from the one represented by Eqn. 8, was introduced in the calculation every 500 cycles in order to surpress hourglass-type mesh motion, using the forth order node coupling approach described by Cloutman et al. [26].

The pressure profile behind the blast wave from Cercion is compared with the self-similar solution in Fig. 11. The self-similar solution was obtained using the technique described by Kamm and Timmes [27]. Cercion calculates a pressure near the origin of 3.6 kbar which is about 5.3% less than the self-similar solution which is shown as the solid line. The density profile is given in Fig. 12. Density profiles moving away from the origin along lines at 90 degrees and 45 degrees from the axial direction are similar in the Cercion calculation. Cercion predicts a peak density of about 3.7 g/cm^3 at the shock front which is about 7.5% less than the value of 4.0 g/cm^3 from the self-similar solution. Differences in symmetry are more evident in the velocity magnitude profile behind the shock presented in Fig. 13. The velocity magnitude at 45 degrees overlaps the analytic solution fairly well in general, but at a distance of about 0.45cm from the origin the velocity magnitude at 45 degrees is noticeably higher than at 90 degrees. The calculated shock front extends slightly beyond the analytic solution and this is most likely due to the fact that starting from an early time in the simulation the total energy is about 2.1% higher than the prescribed initial value. For the duration of the problem the total energy is always within 2.1% of the prescribed initial value.

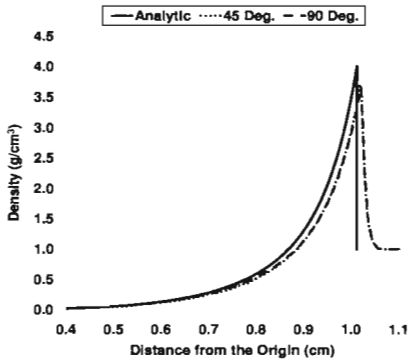

Figure 12: Pressure for the Sedov test problem.

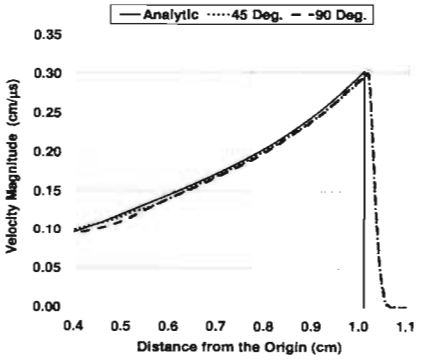

Figure 13: Velocity magnitude for the Sedov test problem.

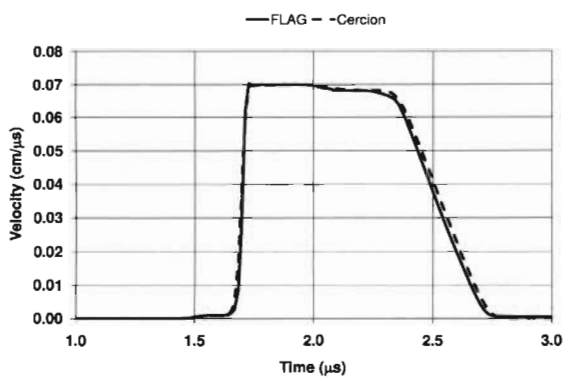

Figure 14: Comparison of the velocity from Cercion (dashed) and FLAG (solid) for the flyer plate test problem.

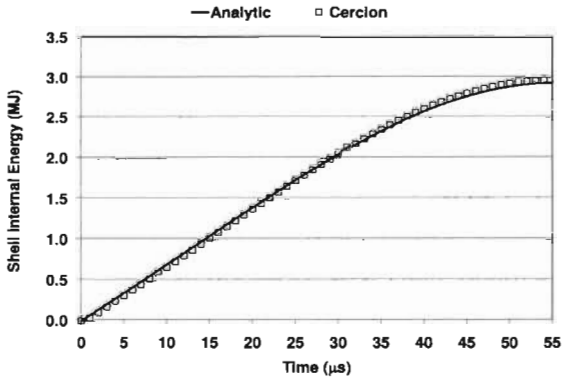

Figure 15: Internal energy for the Verney test problem.

A flyer plate test problem was formulated to evaluate the material strength treatment in Cercion in one dimensional geometry. An aluminum projectile which is 2mm in length containing 40 cells and having a velocity of 0.07 cm/ μs impacts an aluminum target at rest that is 1 cm in length with 200 cells. For this test problem there is no mesh relaxation and the fluid equations are solved in a Langrangian fashion. A Mie-Gruneisen equation of state is used to represent aluminum with the parameters taken from Steinberg [6]. A simple elastic-plastic material strength model is assumed for aluminum with a constant shear modulus of 270 kbar and a constant yield stress of 0.4 kbar. The velocity temporal profile at the target-vacuum interface is presented in Fig. 14. A companion calculation was performed with another Lagrangian code, FLAG. The Lagrangian method in FLAG is distinct from the Cercion method in that the discrete equations of FLAG are formulated to preserve total energy exactly [28]. Both Cercion and FLAG show an elastic precursor wave in the velocity profile starting just before 1.5 μs and lasting for 0.2 μs. There is agreement in peak velocity with both codes giving a value of 0.07cm/ μs, which conforms to the theoretical value for this kind of impact. The duration of the velocity pulse at the target-vacuum interface is the same and in general there is good agreement between the two codes for the release wave.

The test problems in this section have helped establish confidence in the basic equations for the Lagrangian velocity update, Eqn. 1 and Eqn. 2, as well as the calculation of the strain rate components, Eqn. 3 thru Eqn. 6 and the higher order remap algorithm involving Eqn. 10 that utilizes the flux volume centroid method from Eqn. 11 to construct the fluxes.

4. Implosion Test Problems

A more rigorous test of the fidelity of the numerical algorithms presented here for determining the strain rate components and remapping materials across cell boundaries involves the implosion of a steel shell in both spherical and cylindrical geometry. Two test problems are now described that provide insight into how well internal energy is calculated during the implosion. For both test problems a Mie-Gruneisen EOS is used for steel with parameters for stainless steel 304 taken from Steinberg [6]. In addition an elastic-plastic strength model having a constant shear modulus of 895 kbar and a constant yield stress of 50 kbar is applied.

The Verney test problem simulates the spherical implosion of a steel shell with an inner radius of 8.0 cm and a thickness of 0.5 cm. The implosion occurs in a vacuum and the initial velocity distribution is such that the density of the steel shell is constant during the implosion. The initial radial velocity, u, varies with radius, r, such that $u = u_0^2(r_0/r)^2$, where $u_0 = 0.14$cm/μs and $r_0 = 8.0$cm. This initial velocity distribution results in a kinetic energy of 2.93 MJ at the beginning of the problem and as the implosion progress the initial kinetic energy is gradually tranformed into internal energy. An analytic solution for the internal energy of the shell as a function of time can be determined using the approach given by Weseloh [29]. The internal energy calculated by Cercion is given in Fig. 15 and the calculation was performed with 40 zones inside the steel shell. The agreement between the analytic solution and the Cercion calculation is good throughout the duration of the implosion as evident in Fig. 15. At 55 μs Cercion gives an internal energy that is about 1% larger than the analytic result. The internal energy at 55 μs increases to 2% when the resolution in the calculation is reduced

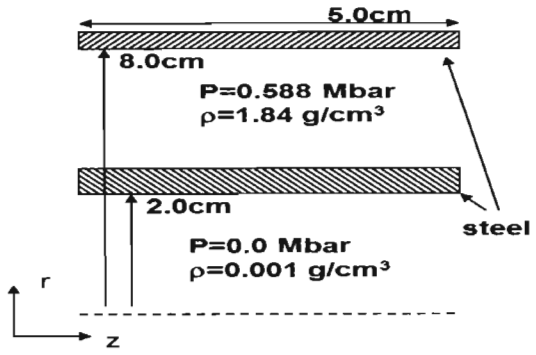

Figure 16: Geometry of the steel test problem.

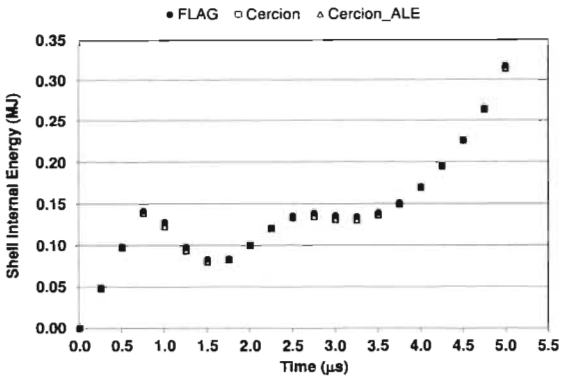

Figure 17: Internal energy for the cylindrical steel implosion.

from 40 zones to 20 zones.

In addition to the Verney problem another good test of energy conservation involves the implosion of a steel shell in converging cylindrical geometry. A simple test problem involving two steel shells, separated by a high pressure gas region was constructed as shown in Fig. 16. The outer steel shell has a thickness of 0.25cm which is spanned by 10 radial zones and the inner shell is 0.5cm thick with 40 radial zones. There are 10 axial zones in the problem and the cylindrical shells are 5 cm long. The high pressure gas region depicted in Fig. 16 contains 80 radial zones and provides the energy to compress the inner steel shell. Contained within the inner shell is a low pressure gas region consisting of 20 radial zones. Both gas regions were represented as ideal gases in the calculations and initialized according to the conditions specified in Fig. 16. Cercion calculations were performed both with and without ALE using a fixed time step of $10^{-3}\mu$s. The simulations lasted 5 μs and a companion FLAG calculation was also performed having the same mesh and time step, using a purely Lagrangian treatment of the hydrodynamics. FLAG and Cercion both give a total energy (internal plus kinetic) of about 2.68 MJ for the inner steel shell at 5 μs. In general the calculated values of total energy are nearly identical with less than a 1% difference between the two codes during the implosion. Maximum compression of the shell occurs shortly after 5 μs. The internal energy calculated during the implosion is presented in Fig. 17 with the FLAG result shown as circles and the Cercion result as squares. An additional Cercion simulation was performed using ALE, such that mesh relaxation occurred at every cycle everywhere except at material boundaries. The Cercion result with ALE is shown as triangles in Fig. 17. It is striking that the use of ALE during the implosion has virtually no effect on the internal energy calculated by Cercion. Although the agreement between FLAG and Cercion is excellent for kinetic energy with regard to internal energy there are some noticeable differences. The Cercion internal energy is approximately 4.5% smaller than the FLAG value at 1.25 μs and 3.6% smaller at 3.0 μs. There is less than a 1% difference in kinetic energy between the two calculations during the implosion with both codes giving a maximum kinetic energy of 2.37 MJ at 5 μs.

5. Summary and Conclusion

Cercion uses proven numerical methods for the solution of the Langrangian equations of motion and the calculation of material strength properties. Cell-centered data structures simplify the programming of the code and allow for efficient memory allocation for multi-material problems. A second-order accurate remap method is used that incorporates monotone derivatives using the Barth-Jesperson technique and constructs material fluxes in a straightforward way by explicitly calculating the true geometric centers of the flux volumes. Results from a series of five test problems indicate that Cercion is robust and its basic algorithms for calculating material strength and remapping materials have been validated.

In general Cercion shows good agreement with the analytic solution when calculating the Sod shock tube problem on a fixed mesh. Compared with other advection methods Cercion is more dissipative and perhaps this can be improved in future work by utilizing a different limiter when calculating the monotone derivatives. There is good symmetry in the Cercion solution for the Sedov blast wave problem. Despite the fact that the

discrete equations of Lagrangian motion are not formulated to conserve total energy in Cercion, nevertheless total energy is conserved to within 2.1% when simulating the Sedov blast wave. In pure Langrangian mode, both Cercion and FLAG give similar velocity profiles at the target-vacuum interface for the flyer plate test problem. This establishes confidence in the numerical implementation of the Margolin strain rate method.

Cercion calculates the internal energy for the Verney problem to within 1% of the analytic solution during the spherical implosion of an incompressible steel shell. For the cylindrical implosion test problem Cercion and FLAG calculate similar total energies for the inner steel shell during the implosion time interval. For cases with and without ALE, Cercion generally gives a similar internal energy for the inner shell as FLAG but during certain portions of the implosion there are differences of no more than 4.5% between the two codes. The kinetic energy of the inner shell, however, is always in very good agreement between the two codes. The Cercion results are insensitive to the use of ALE during the implosion demonstrating that the higher-order remap algorithm presented here does not introduce any meaningful errors in mass, momentum or internal energy during the calculation.

The two implosion test problems presented here provide a rigorous test of energy conservation for ALE methods. Besides the HEMP based Lagrange method in Cercion and the total energy preserving method of FLAG there are a number of distinct Lagrangian hydrodynamic algorithms in the literature. A comparison with some of these other numerical methods would help illustrate how different techniques partition energy between internal and kinetic modes.

6. Acknowledgments

The author wishes to thank Marianne Francois and Nathaniel Morgan for their helpful comments and suggestions. This work was performed under the auspices of the National Nuclear Security Administration of the United States Department of Energy at Los Alamos National Laboratory under contract No. DE-AC52-06NA25396.

References

[1] D. Benson, Computational methods in lagrangian and eulerian hydrocodes, Computer Methods in Applied Mechanics and Engineering 99.

[2] A. A. Amsden, H. Ruppel, C. Hirt, Sale: A simplified ale computer program for fluid flow at all speeds, Technical Report LA-8095, Los Alamos National Laboratory (1980).

[3] C. Hirt, A. Amsden, J. Cook, An arbitrary lagrangian-eulerian computing method for all flow speeds, Journal of Computational Physics 14 (1974) 227–253.

[4] M. Wilkins, Calculation of elastic-plastic flow, Technical Report UCRL-7322, Lawrence Livermore National Laboratory (1963).

[5] D. Preston, D. Tonks, D. Wallace, Model of plastic deformation for extreme loading conditions, Journal of Applied Physics 93.

[6] D. Steinberg, Equation of state and strength properties of selected materials, Technical Report UCRL-MA-106439, Lawrence Livermore National Laboratory (1996).

[7] R. Demuth, L. Margolin, B. Nichols, T. Adams, B. Smith, Shale: A computer program for solid dynamics, Technical Report LA-10236, Los Alamos National Laboratory (1985).

[8] J. Brackbill, J. Saltzman, Adaptive zoning for singular problems in two dimensions, Journal of Computational Physics 46.

[9] A. Winslow, Equipotential zoning of two-dimensional meshes, Technical Report UCRL-7312, Lawrence Livermore National Laboratory (1963).

[10] C. Laney, Computational Gasdynamics, Cambridge University Press, 1998.

[11] L. Margolin, M. Shashkov, Second-order-sign-preserving conservative interpolation (remapping) on general grids, Journal of Computational Physics 184.

[12] T. Barth, Numerical methods for gasdynamics systems on unstructured grids, in: Proceedings of the International School on Theory and Numerics for Conservation Laws, Freiburg/Littenweiler, Germany, 1997.

[13] D. Youngs, An interface tracking method for a 3d eulerian hydrodynamics code, Technical Report 44/92/35, Atomic Weapons Establishment (1984).

[14] M. Kucharik, R. Garimella, S. Schofield, M. Shashkov, A comparative study of interface reconstruction methods for multi-material ale simulations, Journal of Computational Physics 229 (2010) 2432–2452.

[15] N. Morgan, A new liquid-vapor phase transition technique for the level set method, Ph.D. thesis, Georgia Institute of Technology (2005).

[16] J. von Neumann, R. Richtmyer, A method for the numerical calculations of hydrodynamical shocks, Journal of Applied Physics 21 (1950) 232.

[17] R. Bowers, J. Wilson, Numerical Modeling in Applied Physics and Astrophysics, Jones and Bartlett Publishers, 1991.

[18] M. Wilkins, Use of artificial viscosity in multidimensional fluid dynamic calculations, Journal of Computational Physics 36 (1980) 281–303.

[19] R. Christiansen, Godunov methods on a staggered mesh: An improved artificial viscosity, Technical Report UCRL–JC105269, Lawrence Livermore National Laboratory (1991).

[20] D. Youngs, Time-dependent mulit-material flow with large fluid distortion, in: K. Morton, M. Baines (Eds.), Numerical Methods for Fluid Dynamics, 1982, pp. 273–285.

[21] L. Margolin, T. Adams, Spatial differencing for finite difference codes, Technical Report LA-10249, Los Alamos National Laboratory (1985).

[22] G. Sod, Survey of several finite difference methods for systems of nonlinear hyperbolic conservation laws, Journal of Computational Physics 26 (1978) 1–31.

[23] S. Davis, A simplified tvd finite difference scheme via artifical viscosity, SIAM Journal of Scientifc and Statistical Computing 8 (1987) 1–18.

[24] W. Anderson, J. Thomas, B. V. Leer, Comparison of finite volume flux vector splittings for the euler equations, AIAA Journal 24 (1986) 1453–1460.

[25] R. Gentry, R. Martin, B. Daly, An eulerian differencing method for unsteady compressible flow problems, Journal of Computa-

tional Physics 1 (1966) 87–118.

[26] L. Cloutman, J. Dukowicz, J. Ramshaw, A. Amsden, Conchas-spray: A computer code for reactive flows with fuel sprays, Technical Report LA-9294-MS, Los Alamos National Laboratory (1982).

[27] J. R. Kamm, F. X. Timmes, On efficient generation of numerically robust sedov solutions, Technical Report LA-UR-07-2849, Los Alamos National Laboratory (2007).

[28] E. Caramana, D. Burton, M. Shashkov, P. Walen, The construction of compatible hydrodynamics algorithms utilizing conservation of total energy, Journal of Computational Physics 146 (1998) 227–262.

[29] W. N. Weseloh, Pagosa sample problems, Technical Report LA-UR-05-6514, Los Alamos National Laboratory (2007).